Available online at www.sciencedirect.com
SCIENCE DIRECT®
Journal of Solid State Chemistry 177 (2004) 4104–4111
JOURNAL OF SOLID STATE CHEMISTRY
www.elsevier.com/locate/jssc

Percolative small-polarons conduction regime in $Ce_{1-x}Gd_xO_{2-x/2}$, probed by the EPR spectral intensity of Gd^{3+}

Cesare Oliva[a,*], Marco Scavini[a], Omar Ballabio[a,1], Agusti Sin[b], Antonio Zaopo[b], Yuri Dubitsky[b]

[a] *Dipartimento di Chimica Fisica ed Elettrochimica dell, Università degli Studi di Milano, Via C. Golgi 19, 20133 Milan, Italy*
[b] *Pirelli Labs S.p.A., Viale Sarca 222, 20126 Milan, Italy*

Received 6 May 2004; accepted 6 July 2004

Abstract

EPR analysis is carried out with $Ce_{1-x}Gd_xO_{(4-x)/2}$ ($x=0.1$; 0.2) nanopowders aiming at obtaining information about their oxidation and reduction properties. The EPR spectrum of these systems is composed of a single feature. The first derivative peak-to-peak spectral intensity decreases at higher temperatures, but this trend deviates from that of Curie's law with the $x=0.1$ sample, at difference with the $x=0.2$ sample. This unexpected result is related to oxygen deficiency, due to gas–solid equilibrium, present in the former sample only. As a consequence, some Ce^{3+} ions would form providing it with conduction electrons propagating as small polarons in a percolative way. This would result in a thinner skin depth at higher temperatures, able to explain the deviation of the spectral intensity from its expected value. Indeed, this deviation from Curie's law is reduced or disappears at all after thermal treatment of the $x=0.1$ sample with O_2.

Keywords: Nanopowders; Small polarons; Conductivity; EPR of Gadolinium as probe

1. Introduction

In the past years, CeO_2-based materials have been intensively studied as catalysts, structural and electronic promoters for heterogeneous catalytic reactions [1] and oxide ion conducting electrolytes for electrochemical cells [2]. The last goal is what addressed our efforts to develop ceria-based (i.e. $Ce_{1-x}Gd_xO_{(4-x)/2}$, afterwards named CGO) solid electrolytes. These would be characterized by ion conductivity higher than conventional yttria-stabilized-zirconia-based and would be able to operate at lower temperatures (500–700 °C) [3]. At this aim we have adopted a synthesis procedure by wet chemistry, often called the "chemical route". This can overcome many of the disadvantages associated with the ceramic route. Indeed, a more homogeneous product is expected by the chemical route because the reagents mix at molecular level. Moreover this technique allows to obtain nano-structured samples. Therefore, these materials are characterized by a very high specific surface area and, consequently, their thermodynamics can be quite different from that of bulk materials [4] so that different defect equilibria arise in the two cases [5]. This is a key point as defect equilibria determine the amount of charge carriers (oxygen vacancies and/or electrons). On the other hand, only ionic conduction is required in electrolytes for electrochemical cells.

In this paper CGO nanostructured samples have been characterized by EPR spectroscopy. This technique proved a fast tool to evidence the presence, if any, of electron conductivity, and to study its mechanism.

*Corresponding author. Fax: +39-02-503-14300.
E-mail address: cesare.oliva@unimi.it (C. Oliva).
[1] Present address: CORIMAV, Viale Sarca 222, 20126 Milan, Italy.

0022-4596/$ - see front matter © 2004 Elsevier Inc. All rights reserved.
doi:10.1016/j.jssc.2004.07.031

2. Experimental

The $Ce_{1-x}Gd_xO_{2-x/2}$ nanopowders have been produced by acrylamide polymerization process [6,7].

$Ce(NO_3)_3yH_2O$ and $Gd(NO_3)_3zH_2O$ (both 99.9% Aldrich), where y and z have been determined by thermogravimetric analysis, were dissolved separately in water and chelated by the addition of the ethylene-diamino-tetraacetic acid (EDTA) powder (Fluka, 98%). The pH were adjusted with NH_4OH (20%, Carlo Erba) up to complete dissolution ($4 < pH < 5$). The EDTA amount corresponds to the molar stoichiometric ratio 1 mol EDTA: 1 mol cation. This chelation was used to prevent the possible reaction of the acrylamide monomers with the cations, which would inhibit the polymerization process [8,9]. The solutions were mixed in order to obtain the desired cationic ratio (see below). Then 15 g of Acrylamide (Fluka, 99%), 1.5 g of bis-acrylamide (i.e. *N*,*N*′-Methylenebiscrylamide, Fluka, 99%) monomers and the initiator AIBN (i.e. 2,2′-Azobis 2-methylbutyronitrile, Fluka 98%) were added to a 200 ml of solution for polymerization to occur [8,10]. The solution was vigorously stirred and heated up to gel formation (~80 °C). Then the gel was dried and calcined at 600 °C for 2 h in an open alumina crucible in air, obtaining $Ce_{1-x}Gd_xO_{2-x/2}$ samples with $x = 0.1$ and 0.2. Hereafter, we will refer to these samples as "as prepared" CGO10 and CGO20, respectively.

Aliquots of samples of both compositions have been annealed in pure oxygen flux for 40 h at 473 and at 773 K. These samples will be called in the following "473 K" and "773 K oxidized samples", respectively. This procedure produces samples whose defect concentrations are fixed by the thermodynamic conditions of the annealing (T and $P(O_2)$).

Room temperature XRPD patterns were collected between 20° and 80° (2θ range, $\Delta 2\theta = 0.02°$) and counting rate of 1 s/step, with a Philips 1820 diffractometer operating with Ni-filtered Cu–$K\alpha$ radiation. In some cases wider 2θ range ($20 < 2\theta < 105°$) and/or longer counting time (10 s/step) have been used.

Rietveld refinement have been performed using the GSAS software suite [11] and its graphical interface EXPGUI [12]. Background have been subtracted using a fifth-order shifted Chebyshev polynomial. The diffraction peak profile has been fitted with a pseudo-Voight profile function. Site occupancies have been kept constant during the refinement while all isotropic thermal factors have been varied.

The EPR spectra have been recorded by a Bruker Elexsys spectrometer equipped with liquid nitrogen variable temperature device (modulation amplitude 4 G, microwave power 20.07 mW, gain 60 dB). EPR spectra have been recorded in a wide temperature range ($105 < T < 380$ K). Samples containing a probe composed of iron oxides have been also examined, to verify that the sensitivity of the EPR cavity was not changing with the sample temperature.

3. Results

The Rietveld refinement performed on XRPD patterns have revealed that all the samples were monophasic. Only the fluoritic $Ce_{1-x}Gd_xO_{2-x/2}$ phase was apparent (cubic system, space group *Fm-3 m*).

The diffraction pattern relative to the as-prepared CGO10 sample is reported in Fig. 1 as an example. The experimental (crosses) and calculated (continuous line) X-ray patterns are shown in the figure together with the difference profile (bottom). In order to check the presence of impurity phases, long counting times (10 s/step) have been adopted.

Both the absence of foreign-phase reflections and the good statistical parameters obtained for the fit ($wRp = 0.0303$, $Rp = 0.0245$) testify the high quality of the sample.

In nanopowders the broadening of X-ray reflections is mainly due to the small domain size. Thus, the volume weighted crystallite size D_V can been obtained from the Sherrer formula [13]:

$$nD_V = \sum_{j=1}^{n} \frac{\lambda}{\beta_j \cos\theta_j}, \tag{1}$$

where β_j is the integral breadth of the jth Bragg peak centered in $2\theta_j$ (all expressed in radians).

For comparison, D_V has been estimated also from the profile parameters contained in the GSAS refinement, by the relation

$$D_V = \frac{36000\lambda}{\pi^2 LX}, \tag{2}$$

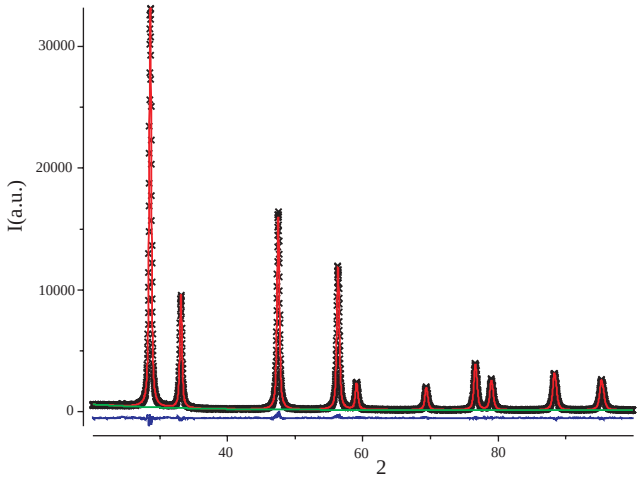

Fig. 1. Observed (crosses) and calculated (continuous line) profile of the "as prepared" CG10 sample. In the same figure the residuals are also shown (bottom).

where LX represents the $1/\cos\theta$ -like contribution to the lorentzian part of the pseudo-Voight profile function [11]. See [14] for a discussion on this method.

Table 1 summarizes the D_V values. In the same table the a crystallographic parameter is shown. The standard deviations of the D_V values obtained from the GSAS refinement are probably underestimated as they derive directly from the standard deviation of the LX parameter. The two methods give very similar results, with an agreement always within two sigma (obtained with the Sherrer formula).

It is apparent that, for each composition, the heat treatment does affect significantly neither the crystallite dimension nor the a parameter. Conversely the gadolinium concentration x seems to affect both D_V and a. In particular the a parameters obtained from the refinements match well with literature results [15]

Fig. 2 shows some selected first-derivative EPR spectra, as an example. In particular, Fig. 2A shows the EPR spectra of CGO10 and CGO20 "as prepared" samples at the same temperature (110 K). Figs. 2B and C show the EPR spectra of CGO10 and CGO20 "as prepared" samples, respectively, at two different temperatures (110 and 380 K).

All spectra show a single $g \cong 2.02$ EPR feature independently from composition, annealing procedure and temperature.

The first-derivative peak-to-peak line intensity I was 1.5 times larger for CGO10 than for CG20; the peak-to peak line-width ΔH_{pp} was smaller with the former than with the latter sample at all the detected temperatures (see for example Fig. 2A). The spectral shape was approximately Lorentzian, but the left part of this feature was always a bit broader than the right one. Attempts to better simulate these spectra with anisotropic hamiltonian parameters or as sum of two Lorentzian-shaped lines led to ambiguous results, due to the line broadness. However, we have verified that no change of line shape or width occurred with the temperature. Therefore, in the present investigation the only spectral parameter taken into account has been the spectral intensity.

The trends of I vs. T are shown in Fig. 3 for the "as prepared" CGO10 sample (triangles), and after its

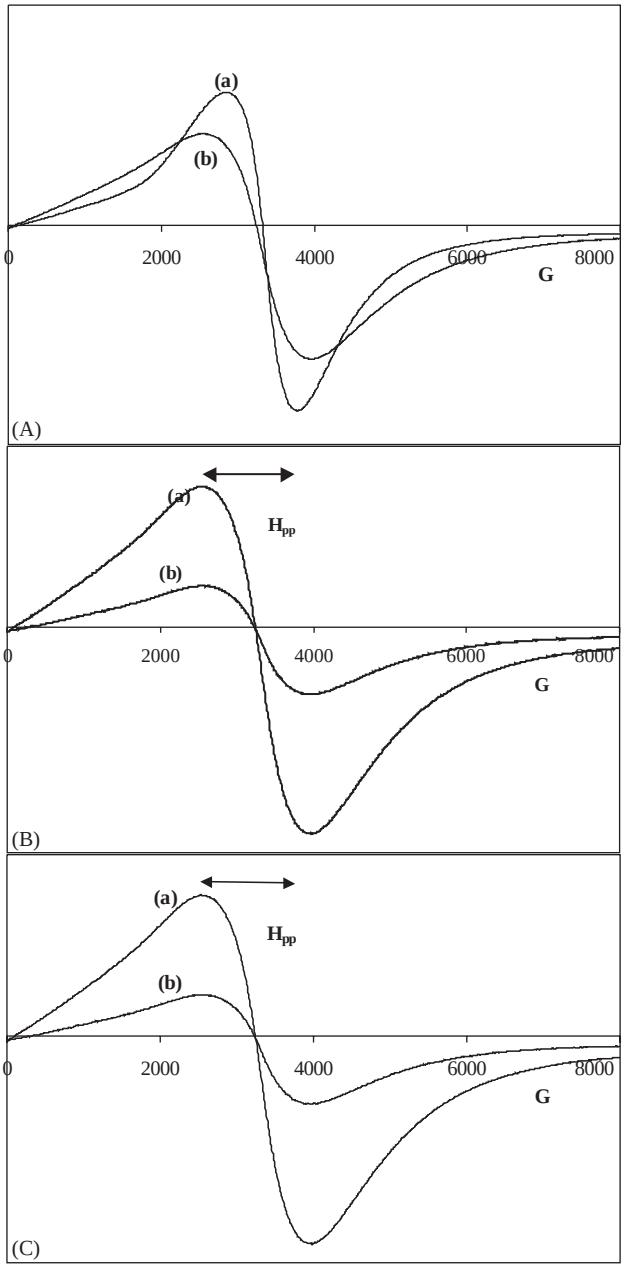

Fig. 2. EPR spectra of "as prepared" $Ce_{1-x}Gd_xO_{(4-x)/2}$. (A) (a) CGO10 and (b) CGO20 samples at 110 K. (B) CGO10 sample at (a) $T = 110$ K and (b) 380 K ($\Delta H_{pp} = 880$ K). (C) CGO20 sample at (a) $T = 110$ K and (b) at 380 K ($\Delta H_{pp} = 1300$ K).

Table 1
Volume weighted crystallite size D_V for the two samples after the different heat treatments

Sample	Parameter	As prepared	Oxidized at 473 K	Oxidized at 773 K
$Ce_{0.9}Gd_{0.1}O_{1.95-\beta}$	D_V (Å): Sherrer method	180(12)	197(12)	193(11)
	D_V (Å): LX method	198(1)	204(1)	209(1)
	a (Å)	5.4198(1)	5.419(1)	5.4186(2)
$Ce_{0.8}Gd_{0.2}O_{1.90}$	D_V (Å): Sherrer method	88(5)	86(5)	86(8)
	D_V (Å): LX method	85(1)	86(1)	84(1)
	a (Å)	5.424(3)	5.427(3)	5.4261(7)

Note. The crystallographic constants a are also shown.

oxidation at 473 K (circles) and at 773 K (squares) in pure oxygen. The trend of the spectral intensity $I(T)$ vs. T is described by $I(T)/I(110\,\mathrm{K}) \propto T^{-1+\alpha}$ (continuous lines in Fig. 3). The meaning of the equation and of α parameter will be discussed in the following section. Table 2 summarizes the EPR results. As a final remark, the same EPR measurements have been performed 1 year later on all the samples to test their stability; results indistinguishable from the previous ones have been obtained.

4. Discussion

4.1. EPR spectral intensity vs. T and conductivity

Gd^{3+} ions showed a single EPR feature also in many literature cases [16–20]. A Lorentzian-shaped EPR line was reported for $GdBa_2Cu_3O_7$ [16], $Gd_{0.5}RE_{0.5}Ba_2Cu_3O_{7-\delta}$ (R = Y, Sm, Eu) [18] and $Gd_{2-x}Ce_xCuO_4$ [19] with line-width independent of temperature in the temperature range examined also in this work.

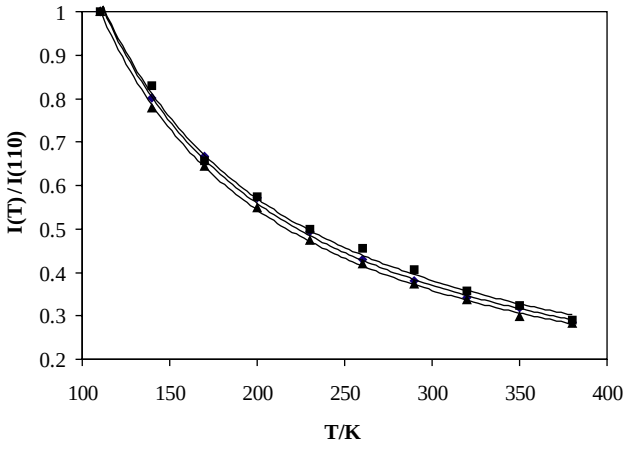

Fig. 3. Peak-to-peak first derivative EPR spectral intensity $I(T)$ divided by its value at $T = 110$ K vs T. CG10 sample. Lowest curve: O_2 untreated sample. Intermediate curve: after oxidation with O_2, carried on at 473 K for 40 h. Upper curve: after oxidation with O_2, carried on at 773 K for 40 h. Continuous lines: best fits of the experimental data (see text and Table 1).

The Gd^{3+} EPR line broadened by doping $GdBa_2Cu_3O_7$ with Co or Ni [16] or with Fe [17]. This was attributed to a reduction of the spin–spin relaxation time T_2 of Gd^{3+} due to its interaction with the doping paramagnetic ions.

In the present investigation, the EPR line is broader for sample CGO20 than for sample CGO10, i.e. with increasing gadolinium concentration; this suggests that Gd^{3+} ions interact to each other, causing a shorter T_2 value at higher Gd^{3+} concentration.

The peak-to-peak first-derivative spectral intensity I decreased with increasing temperature with both samples, while the peak-to-peak line width ΔH_{pp} and the spectral profile remained unchanged. Therefore, these changes of I are attributable to variations of the paramagnetic susceptivity χ of the sample.

In a system of non-interacting paramagnetic ions, χ and so also $I(T)$ vary with the temperature following the Curie's law:

$$I(T)T = I_{110\,\mathrm{K}}, \tag{3}$$

where 110 K is the lowest measured temperature.

Deviations from the Curie law can be described by

$$I(T)T = I_{110\,\mathrm{K}}T^{\alpha}. \tag{4}$$

α is greater than 0 in the presence of magnetic interactions among paramagnetic ions. This leads to an increase of $I(T)T$ with T [21]. An opposite effect, i.e. a decrease of $I(T)T$ vs. T ($\alpha < 0$), has been attributed to thermally activated electronic conductivity σ due to small polarons hopping between ions in different valence states [18,20]. In fact, when an electronic contribution to conductivity is present it causes a "skin depth" if the sample undergoes a microwave magnetic field of frequency ω. If σ increases with increasing

Table 2
EPR spectral parameters with $Ce_{1-x}\,Gd_x\,O_{(4-x)/2}$

Sample	x	g	ΔH_{pp} (G)	I (a.u.) (different at each T)	I(105 K)/I(380 K)	α in: $I(T)/I(100\,\mathrm{K}) \sim T^{-1+\alpha}$		
						As prepared	$P(O_2) = 1$ atm at 473 K[a]	$P(O_2) = 1$ atm at 773 K[a]
CGO10	0.1	≅2.02	880	$1.5 \times I_{P23}$	3.2	−0.026 ±0.009 $R^2 = 0.9994$	−0.01 ±0.01 $R^2 = 0.9984$	+0.01 ± 0.02 $R^2 = 0.9962$
CGO20	0.2	≅2.02	1300	$I_{P23}(T)$	3.2	+0.02 ±0.02 $R^2 = 0.9967$	+0.03 ±0.02 $R^2 = 0.9964$	+0.04 ±0.01 $R^2 = 0.9995$

Note. Not ox = sample not oxidised.
[a]Temperature at which a sample oxidation with O_2 has been carried on for 40 h.

temperature, a thinner "skin depth" will arise and then the EPR signal intensity will get lower than expected on the basis of the Curie law ($\alpha<0$). A detailed description of this phenomenon is reported in the Appendix.

This phenomenon, i.e. a negative α value, is observed only with the "as prepared" and "oxidized at 473 K" CGO10 samples (see Table 2); indeed in the latter case the standard error on α has the same value of α itself, so that α cannot be safely evaluated. Fig. 4 shows the plot of $I(T)T$ vs. T for these two samples. The parameter α is positive for the CGO10 sample oxidized at 773 K and for the CGO20 sample independently from the annealing procedure. Both the annealing conditions and the doping level seem to be crucial in order to obtain (or to avoid) electronic conduction. This will be easily interpreted in the framework of defect equilibria in the next paragraph. However, EPR cannot provide the absolute value of bulk conductivity (see the Appendix), but it appears as a direct and fast probe of the presence of electronic conductivity on a given sample.

4.2. Defect equilibria and electronic transport

If we consider the fluorite-type CeO_2 structure as reference structure, the relevant defect equilibria, in the Kröger–Vink notation [22], are

$$Gd_2O_3 \rightarrow 2Gd'_{Ce} + 3O_O + V_O^{\bullet\bullet} \quad (5)$$

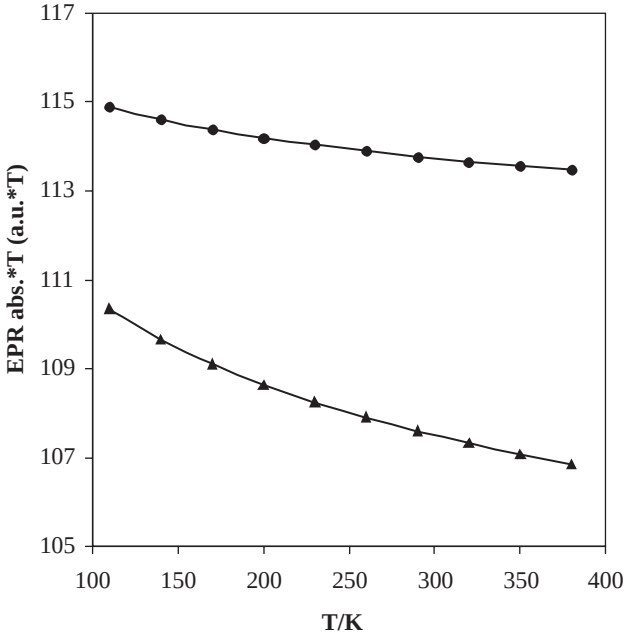

Fig. 4. Peak-to-peak first derivative EPR spectral intensity $I(T)$ multiplied by temperature T vs T. From bottom to top: CGO10 not treated with O_2; the same sample after oxidation with O_2 at 473 K.

for gadolinium doping and

$$O_O \rightleftarrows \frac{1}{2}O_2 + 2e' + V_O^{\bullet\bullet} \quad (6)$$

for oxygen equilibrium with atmosphere.

It must be noted that the concentration of oxygen vacancies introduced by equilibrium (5) is fixed by the synthesis whereas the concentration of oxygen vacancies introduced by equilibrium (6) depends on the thermodynamic conditions [T and $P(O_2)$] of the annealing.

We can neglect the intrinsic formation and annihilation of electrons and holes because of the wide energy gap between the valence and the conduction band (2.5 eV for pure CeO_2 [23]). Therefore, we can write the following electroneutrality equation:

$$[Gd'_{ce}] + [e'] = 2[V_o^{\bullet\bullet}] \quad (7)$$

where $[e']$ is the concentration of electrons in the conduction band, where electrons are introduced when the concentration of oxygen vacancies per formula exceeds $x/2$. Thus, we can write the chemical formula of the samples putting in evidence the contributions of equilibria (5) and (6) to the oxygen non-stoichiometry, i.e. as $Ce_{1-x}Gd_xO_{2-x/2-\beta}$, where β is a function of x, T and $P(O_2)$.

Eqs. (6) and (7) can be combined to obtain the following equilibrium:

$$\begin{aligned} K(T) &= [V_O^{\bullet\bullet}] \cdot [e']^2 P(O_2)^{1/2} \\ &= \frac{[Gd'_{Ce}] + [e']}{2}[e']^2 P(O_2)^{1/2} \\ &\approx \frac{[Gd'_{Ce}]}{2}[e']^2 P(O_2)^{1/2}. \end{aligned} \quad (8)$$

$[e']$ increases when oxygen partial pressure or/and gadolinium concentration x decreases. On the other hand the electronic conductivity is proportional to $[e']$, being:

$$\sigma = [e']q\mu(T), \quad (9)$$

where $\mu(T)$ is the carrier mobility and q is the electronic charge.

Only the "as prepared" CGO10 sample shows clearly electronic conduction; so, in this case, $\beta(>0)$ deviates significantly from 0; β seems to be circa 0 for CGO10 in the remaining annealing condition and for CGO20 sample in all the annealing conditions. Therefore all the EPR experimental results, being related to σ, are interpreted by the defect equilibria (see Eq. (8)). The last, in turn, depend on the particle size.

All the investigated samples are nanocrystalline, as shown by XRPD results. In particular, the volume weighted crystallite size D_v is ~190 Å for CGO10 and ~90 Å for CGO20 samples. The role of nanosize on the defect equilibria in this system can be evaluated by comparing our results with the ones obtained on coarser samples by means of impedance spectroscopy (IS).

IS measurements have been performed on micrometric CeO_2 [5] and $Ce_{1-x}Gd_xO_{2-x/2}$ [24,25] samples at T and $P(O_2)$ conditions similar to those adopted in our annealing. Gadolinium-doped ceria showed only ionic conduction [24,25].

Thus nanosize increases vacancies concentration with respect to non-nanometric samples. This effect seems to be due to a strong decrease of the heat of reduction in nanometric samples ($\Delta H_R = 1.84$ eV for CeO_2 [4]) with respect to samples with coarser grain size ($\Delta H_R = 4.7$ eV [26]). IS measurements performed on $Ce_{1-x}Gd_xO_{2-x/2}$ nanometric samples [4,25] are in accordance with the present EPR results.

A comparison between information given by EPR and IS is required. The latter is able to separate bulk, grain boundary and electrode contributions to impedance. In particular, electronic and ionic bulk conductivity can be distinguished if measurements are performed at a fixed temperature in a broad $P(O_2)$ interval. In fact, when β is negligible, only ionic conductivity is apparent and $\sigma[P(O_2)]$ is constant at constant temperature. On the contrary, when β is not negligible, both $[e']$ and σ increase with decreasing $P(O_2)$ (see Eqs. (8) and (9)). Therefore, at difference with EPR, IS needs measurements in a wide range of $P(O_2)$ to determine the presence of electronic contribution to electrical conductivity. Moreover, in the case of nanostructured systems, IS needs a method to compact samples without changing the grain dimensions. By contrast this is not needed with EPR measurement.

4.3. Transport mechanism

It is well known that electronic conduction is achieved via an adiabatic small-polaron hopping mechanism in pure $CeO_{2-\beta}$ [27], the electron mean free path being on the order of atomic separation [5]. The electronic transport mechanism is independent from the grain size [4,5] and from Gadolinium doping [25]. The relevant conductivity equation to describe that type of conduction mechanism is:

$$\sigma = \frac{\sigma_0}{T}\exp\left(-\frac{E_h}{kT}\right), \tag{10}$$

where E_h is the hopping energy.

It is worth noting that all the measurements here quoted have been collected at temperatures above 773 K [28] (i.e. $T > 1/2\theta_0$; θ_0 being the Debye temperature), where the diffusive regime applies for small polarons [29]. At lower temperatures the conductivity deviates from Eq. (10). In ordered systems the polaron behaves like a heavy particle in a band [30], while in disordered systems charge is transported through a "percolative path", i.e. via tunnelling between localized states which are randomly distributed in energy and position [31]. In this latter case, the relevant equation for conductivity is [31]

$$\sigma = \sigma_0 \exp\left[\left(-\frac{T_0}{T}\right)^{\frac{1}{4}}\right]. \tag{11}$$

The conductivity data, obtained by EPR for the "as prepared" sample (full circles), are plotted as $\ln(\sigma)$ vs $T^{-1/4}$ in Fig. 5. In the same figure, the data relative to the "oxidized at 473 K" sample (empty circles) are also shown. However, we remind that the α values is not statistically significant in the latter case.

It is apparent that the data fit well the model described above in the whole temperature range (110 K < T < 380 K). Conversely the results are not compatible with a diffusive conduction mechanism (see Eq. (10)). The dotted regression lines in the insert are guides for the eyes produced by using high temperature data (290 K < T < 380 K).

The use of a $T^{-2/5}$ law [31] or the introduction of a pre-exponential temperature-dependent factor [32] gives similar results, but with slightly worse statistical parameters. It is worth noting that a percolative conduction mechanism is expected at low temperature for this system, as gadolinium doping introduces a great extent of local structural disorder [33,34].

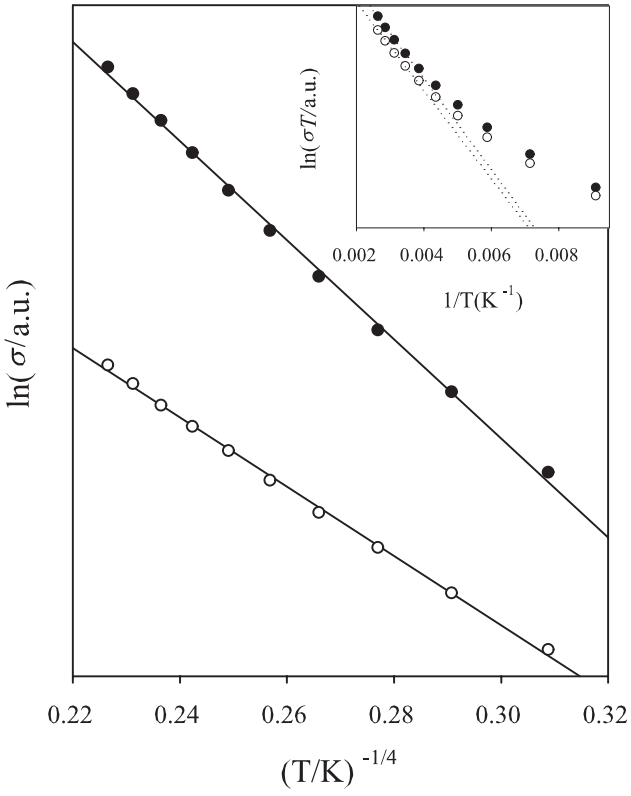

Fig. 5. Plot of $\log\sigma$ vs $T^{-1/4}$ (percolative regime) for the "as prepared" (full circles) and the oxidized at 447 K (empty circles) CGO10 samples (empty circles). Insert: plot of $\log\sigma\ T$ vs T^{-1} for the same samples.

5. Conclusions

The trend of the EPR spectral intensity vs. temperature indicates that the correct formula of "as prepared" CGO10 sample is $Ce_{0.9}Gd_{0.1}O_{1.95-\beta}$ with $\beta>0$. In this compound the oxygen-deficienct β is compensated by electrons in the conduction band. As a consequence an electronic conductivity is acquired by this sample, through a small-polarons percolative regime, in the investigated temperature interval.

A sample oxidation carried out at 773 K for 40 hours eliminates the oxygen deficiency and, therefore, the electronic conductivity.

On the contrary β is circa 0 for sample CGO20 independently from annealing procedure. Thus the correct formula is $Ce_{0.8}Gd_{0.2}O_{1.90}$. Indeed, this sample shows no electronic conductivity even before its oxidation.

EPR spectroscopy is a direct and fast tool to evidence the presence and to identify the mechanism of electronic conductivity.

Acknowledgments

Dr. Serena Cappelli and Dr. Andrea D'Ambrosio, of our department, are acknowledged for their kind technical support.

Appendix

The "skin depth" $\delta(T)$, in the microwave magnetic field of frequency ω, is connected to the electronic conductivity $\sigma(T)$ through the equation

$$\delta(T)=\left[\frac{2}{\mu_0\omega\sigma(T)}\right]^{1/2}, \tag{A.1}$$

where μ_0 is the magnetic permeability in vacuum.

Therefore, the microwave magnetic field penetrates less deeply the sample with increasing $\sigma(T)$, causing an intensity $I(T)$ of the EPR spectrum lower than the value $I_0(T)$ expected on the basis of the Curie's law only. This is the case of samples with thermally activated electronic conductivity σ, characterized by $\alpha<0$ in Eq. (4) [18,20], as in the present case. Furthermore, in this situation $I(T)$ and $I_0(T)$ are connected to each other through the relation [18,35]:

$$I(T)=I_0(T)\frac{2\exp(-w)+[1-\exp(-2w)]/w}{[1+\exp(-w)]^2}, \tag{A.2}$$

where $w=d/\delta(T)$ and $d\,(=3\,\text{mm})$ is the thickness of the sample and the spectral intensities are in arbitrary units.

Therefore, we can express all $I(T)$ and $I_0(T)$ values as a ratio between their value at T and that at a reference temperature (110 K in the present investigation). $I_0(T)$ is calculated in the whole temperature interval by applying the Curie's law. At each temperature T the ratio $I(T)/I_0(T)$ leads to the evaluation of w (Eq. (A.2)), and then of $\delta(T)$. Finally, $\sigma(T)$ can be calculated by substituting $\delta(T)$ into Eq. (A.1). The above procedure does not lead to the evaluation of the actual conductivity but to the ratio between its value at T and that at a reference temperature (the lowest measured one in the present case).

Finally, it is worth noting that the microwave conductivity $\sigma(T)$ is purely real [36] and so, in the absence of superconductivity, it is proportional to DC conductivity.

References

[1] A. Tschöpe, W. Liu, M. Flytzani-Stephanopulos, J.Y. Ying, J. Catalysis 157 (1995) 42–50.
[2] H. Inaba, H. Tagawa, Sol. State. Ionics 83 (1996) 1–16.
[3] B.C.H. Steel, in: H.L. Tuller, J. Schoonman, I. Riess (Eds.), Oxygen Ion and Mixed Conductors and their Technological Applications, NATO ASI Series, Serie E: Applied Sciences 368 (1997) pp. 323–345.
[4] J.-H. Hwang, O. Mason, Z. Physikalische Chemie. 207 (1998) 21–38.
[5] Y.-M. Chiang, E.B. Lavik, I. Kosacki, H.L. Tuller, J.Y. Ying, Appl.Phys.Lett. 69 (1996) 185–187.
[6] T. Tanaka, Sci. Am. 244 (1981) 124–136, 138.
[7] A. Ravve, Principles of Polymeric Chemistry, Kuwer Academic, New York, 2000, p.46.
[8] A. Sin, P. Odier, Advanced Materials 12 (2000) 649–652.
[9] A. Sin, P. Odier, M. Núñez-Regueiro, Physica C 330 (2000) 9–18.
[10] A. Sin, B. El Montaser, P. Odier, F. Weiss, J. Am. Cerm. Soc. 85 (2002) 1928–1933.
[11] A.C. Larson e, R.B. Von Dreele, GSAS: General Structural Analysis System, Los Alamos National Laboratory, Los Alamos, NM, 1994.
[12] B.H. Toby, J. Appl. Cryst. 34 (2001) 210–214.
[13] D. Balzar, S. Popovic, J. Appl. Cryt. 29 (1996) 16–23.
[14] P. Karen, P.M. Woodward, J. Solid State Chem. 141 (1998) 78–88.
[15] Y. Ikuma, K. Takao, M. Kamiya, E. Shimada, Mat. Sci. Eng. B 99 (2003) 48–51.
[16] F. Nakamura, K. Senoh, T. Tamura, Y. Ochiai, Y. Narahara, Physica C 162–164 (1989) 1287–1288.
[17] H. Shimizu, J. Arai, M. Mita, Physica C 162–164 (1989) 1293–1294.
[18] N. Guskos, G.P. Triberis, V. Lykodimos, W. Windsch, H. Metz, A. Koufoudakis, C. Mitros, H. Gamari-Seale, D. Niarchos, Phys. Stat. Sol. (b) 166 (1991) 233–240.
[19] H. Shimizu, S. Suzuki, K. Hatada, Physica C 282–287 (1997) 1379–1380.
[20] N. Guskos, J. Kuriata, I.H. Salikhov, J. Phys. C: Solid State Phys 17 (1984) 2175–2180.
[21] N. Guskos, V. Likodimos, J. Typek, M. Wabia, H. Fuks, Physica C 341–348 (2000) 573–574.
[22] F.A. Kröger, H. Stieltjes, H.J. Vink, Philips Res. Repts. 14 (1959) 557–589.
[23] N.V. Skorodumova, R. Ahuja, S.I. Simak, I.A. Abrikosov, B. Johansson, B.I. Lundqvist, Phys. Rev. B 64 (115108) (2001) 1–9.
[24] M. Mogensen, T. Lindegaard, U.R. Hansen, G. Mogensen, J. Electrochem. Soc. 141 (1994) 2122–2128.

[25] Y.-M. Chiang, E.B. Lavik, D.A. Blom, NanoStructured Materials 9 (1997) 633–642.
[26] H.L. Tuller, A.S. Nowick, J. Electrochem. Soc. 122 (1975) 255–259.
[27] H.L. Tuller, A.S. Nowick, J. Phys. Chem. Solids 38 (1977) 859–867.
[28] I.K. Naik, T.Y. Tien, J. Phys. Chem. Solids 39 (1978) 311–315.
[29] T. Holstein, Ann. Phys. 8 (1959) 343–389.
[30] I.G. Austin, N.F. Mott, Adv. Phys. 18 (1969) 41–102.
[31] G.P. Triberis, L.R. Friedman, J. Phys. C: Solid State Phy. 14 (1981) 4631–4639.
[32] V. Dallacasa, R. Feduzi, Physica C 251 (1995) 156–164.
[33] T. Ohashi, S. Yamazaki, T. Tokunaga, Y. Arita, T. Matsui, T. Harami, K. Kobayashi, Solid State Ionics 113–115 (1998) 559.
[34] T. Nakagawa, T. Osuki, T.A. Yamamoto, Y. Kitauji, M. Kano, M. Katsura, S. Emura, J. Synchrotron Rad 8 (2001) 740–742.
[35] M. Godlewski, H. Przybylinska, J.M. Langer, Appl. Phys. A 30 (1983) 105–107.
[36] H.M. Cheah, A. Porch, J.R. Waldram, Physica B 165/166 (1990) 1195–1196.